

RESEARCH

Open Access



The microvascular extracellular matrix in brains with Alzheimer's disease neuropathologic change (ADNC) and cerebral amyloid angiopathy (CAA)

Mamatha Damodarasamy^{1,2}, Robert B. Vernon³, Jasmine L. Pathan¹ , C. Dirk Keene⁴ , Anthony J. Day⁵ , William A. Banks^{1,2} and May J. Reed^{1,2,6*} 

Abstract

Background: The microvasculature (MV) of brains with Alzheimer's disease neuropathologic change (ADNC) and cerebral amyloid angiopathy (CAA), in the absence of concurrent pathologies (e.g., infarctions, Lewy bodies), is incompletely understood.

Objective: To analyze microvascular density, diameter and extracellular matrix (ECM) content in association with ADNC and CAA.

Methods: We examined samples of cerebral cortex and isolated brain microvasculature (MV) from subjects with the National Institute on Aging-Alzheimer's Association (NIA-AA) designations of not-, intermediate-, or high ADNC and from subjects with no CAA and moderate-severe CAA. Cases for all groups were selected with no major (territorial) strokes, ≤ 1 microinfarct in screening sections, and no Lewy body pathology. MV density and diameter were measured from cortical brain sections. Levels of basement membrane (BM) ECM components, the protein product of TNF-stimulated gene-6 (TSG-6), and the ubiquitous glycosaminoglycan hyaluronan (HA) were assayed by western blots or HA ELISA of MV lysates.

Results: We found no significant changes in MV density or diameter among any of the groups. Levels of BM laminin and collagen IV (col IV) were lower in MV isolated from the high ADNC vs. not-ADNC groups. In contrast, BM laminin was significantly higher in MV from the moderate-severe CAA vs. the no CAA groups. TSG-6 and HA content were higher in the presence of both high ADNC and CAA, whereas levels of BM fibronectin and perlecan were similar among all groups.

Conclusions: Cortical MV density and diameter are not appreciably altered by ADNC or CAA. TSG-6 and HA are increased in both ADNC and CAA, with laminin and col IV decreased in the BM of high ADNC, but laminin increased in moderate-severe CAA. These results show that changes in the ECM occur in AD and CAA, but independently of one another, and likely reflect on the regional functioning of the brain microvasculature.

Keywords: Human neuropathology, Alzheimer's disease, Cerebral amyloid angiopathy, Vascular density, Vascular diameter, Laminin, Collagen IV, Fibronectin, Perlecan, TSG-6, Hyaluronan

*Correspondence: mjr@uw.edu

¹ Division of Gerontology and Geriatric Medicine, Department of Medicine, University of Washington, Seattle, WA, USA

Full list of author information is available at the end of the article



© The Author(s) 2020. This article is licensed under a Creative Commons Attribution 4.0 International License, which permits use, sharing, adaptation, distribution and reproduction in any medium or format, as long as you give appropriate credit to the original author(s) and the source, provide a link to the Creative Commons licence, and indicate if changes were made. The images or other third party material in this article are included in the article's Creative Commons licence, unless indicated otherwise in a credit line to the material. If material is not included in the article's Creative Commons licence and your intended use is not permitted by statutory regulation or exceeds the permitted use, you will need to obtain permission directly from the copyright holder. To view a copy of this licence, visit <http://creativecommons.org/licenses/by/4.0/>. The Creative Commons Public Domain Dedication waiver (<http://creativecommons.org/publicdomain/zero/1.0/>) applies to the data made available in this article, unless otherwise stated in a credit line to the data.

Background

Alzheimer's disease (AD) neuropathologic change (ADNC) is defined by histologic criteria of amyloid- β (A β) and tau deposition throughout brain regions, which are validated and subject to periodic re-evaluation [1, 2]. Cerebral amyloid angiopathy (CAA), a related disease that is also characterized by established histologic criteria, refers specifically to the deposition of A β in the media and adventitia of small and mid-sized arteries (and, much less frequently, veins) of the cerebral cortex and the leptomeninges. In most cases of CAA there is some level of ADNC, but the converse is not true, since many brains with ADNC do not have significant CAA. This distinction has clinical significance in that CAA is an independent risk factor for microaneurysms and intraparenchymal hemorrhages [3, 4].

Study of the microvasculature in aging is complicated by reductions in vessel density (thought due to rarefaction), a thickening of the vascular wall that reflects changes in basement membrane (BM) structure, and poorly characterized alterations in the glycocalyx [5–8]. Consequently, attribution of changes in brain microvasculature (MV) specifically to ADNC or CAA is confounded by the associated factors of advanced age, and other neuropathology that increases with aging such as Lewy bodies, strokes, and microinfarcts [9, 10]. As a result, studies focusing specifically on the vascular changes in AD and CAA have generated conflicting results with respect to blood vessel density, morphology, and associated extracellular matrix (ECM) [11, 12].

The BM of brain MV is an ECM of unique composition at the abluminal surface of vascular endothelial cells, which provides a dynamic interface for cell-ECM communication. The thickness of the normal BM is approximately 40–100 nm and consists of at least four major ECM proteins: laminin, collagen IV (col IV), fibronectin, and nidogen [13]. Also present in the BM are heparan sulfate proteoglycans (HSPGs), such as perlecan and agrin. Laminin and col IV are the dominant components in terms of content and provision of structural support. BM organization begins with deposition of laminin, which interacts with cells (primarily via integrins) to polymerize and bind to less highly expressed ECM components, such as perlecan and fibronectin. The final steps in BM assembly are mediated primarily by col IV, a highly expressed collagen that becomes organized into a 3-dimensional network that stabilizes the structure of the BM [14]. Previous studies of changes in BM ECM in AD and CAA neuropathology have yielded variable results in human and animal models [15–18].

Hyaluronan (HA) is a ubiquitous non-sulfated glycosaminoglycan (GAG) that is constitutively secreted as a large linear polymer throughout the vascular glycocalyx

and the gray and white matter of the brain parenchyma [13]. HA synthesis and turnover is accelerated during injury, resulting in greater amounts of lower MW HA [19]. Whereas high molecular weight HA binds to the highly expressed CD44 receptor, smaller forms of HA are effective competitors of these interactions [20, 21]. It has also been reported that low molecular weight HA interacts directly with CD44 or toll-like receptors to promote inflammation [22–25]; however, at least some of these effects have been attributed to lipopolysaccharide (LPS) contamination in the HA preparations used [26]. HA is usually present in complex with HA-binding proteins (hyaladherins) that together play a critical role in tissue organization and structure; e.g. such as the specialized glycocalyx of perineuronal nets [21]. One such hyaladherin, TSG-6, while only expressed in response to inflammation in most tissues, is constitutively present in the brain ECM [27, 28]. In this context, TSG-6 likely organizes HA molecules into a crosslinked network and plays a protective role in response to brain injury/inflammation [27, 29, 30]. Our previous studies have found greater amounts of HA and TSG-6 in brains with high ADNC relative to those with no ADNC [31].

We wished to determine whether the density, morphology, and ECM content of MV differ in cortical brain tissues with advanced ADNC or CAA. In the present study, we compared age-matched human brain samples, lacking or with varying degrees of either ADNC and CAA, with respect to MV density, MV diameter, and MV ECM composition. AD brain samples were obtained from the parietal cortex of human subjects with not-, intermediate-, or high ADNC. Brain samples with CAA were obtained from the occipital cortex of human subjects divided into two groups: no CAA/not AD and moderate-severe CAA/intermediate-high AD. None of the specimens had significant concurrent vascular or Lewy body neuropathology.

Methods

Brain tissue samples

Samples of human brain tissue were obtained from the tissue repository of the University of Washington Neuropathology (UW NP) Core, where fresh samples are collected within 8 h of death (post-mortem interval = PMI) and rapidly preserved by flash freezing in liquid N₂. Non-frozen samples from short PMI subjects, and all tissues from subjects with > 8 h PMI, were fixed in 10% neutral-buffered formalin, sampled, processed, and then embedded in paraffin (formalin-fixed, paraffin-embedded, FFPE) according to routine protocols (Table 1).

Two groups were studied: one set was comprised of parietal lobe samples that focused on AD pathology ("AD samples"), whereas the second set consisted of occipital lobe samples focused on CAA pathology ("CAA

Table 1 Samples for IHC {paraffin embedded} and biochemistry {frozen}

| | AD brain samples | | |
|------------------|-------------------|----------------|------------|
| | Not AD | Int AD | High AD |
| Female samples | {8} [4] | {7} [5] | {23} [19] |
| Mean age (range) | 81 (71–88) | 86 (72–92) | 88 (70–99) |
| Male samples | {13} [8] | {11} [8] | {17} [13] |
| Mean age (range) | 85 (73–95) | 89 (77–100) | 83 (67–96) |
| | CAA brain samples | | |
| | No CAA | Mod-Severe CAA | |
| Female samples | {7} [7] | {14} [14] | |
| Mean age (range) | 86 (77–98) | 81 (59–98) | |
| Male samples | {7} [7] | {12} [12] | |
| Mean age (range) | 85 (64–101) | 82 (43–96) | |

Table shows sex and age distribution for samples available for histology {paraffin embedded} and biochemistry {frozen} at the time of death

Int AD= Intermediate AD, Mod-Severe CAA= moderate-severe CAA

samples”). For the AD samples, we chose to examine parietal cortex (inferior parietal lobule) as a region exemplifying AD pathologic progression by A β plaques and neurofibrillary tangles. Cases were selected based on the level of ADNC for neuritic plaque density (CERAD score) and neurofibrillary tangle distribution (Braak stage) in subjects with no Lewy body pathology and no more than 1 microinfarct in standard screening sections [2]. Graded levels of A β and tau pathology in parietal cortex samples were confirmed by a board-certified neuropathologist at the original autopsy, using an adaptation of NIA-AA guidelines for CERAD neuritic plaque density and Braak stage for neurofibrillary tangle distribution as assessed by Bielschowsky silver stain and immunostains for hyperphosphorylated tau (pTau), respectively [32]. Since Thal phase was not available for all research participants, levels of ADNC in the samples were classified as “not ADNC” (CERAD=0, Braak=0–II, $n=21$ FFPE/12 frozen); “intermediate ADNC” (CERAD=2, Braak=III–IV, $n=18$ FFPE/13 frozen); and “high ADNC” (CERAD=3, Braak=V–VI, $n=40$ FFPE/32 frozen). Female/male representation was 38%/62% (not ADNC), 39%/61% (intermediate ADNC) and 57%/43% (high ADNC), with an age range of 71–95 years (not ADNC), 72–100 years (intermediate ADNC) and 67–99 years (high ADNC). Patients in the high ADNC group did not differ significantly from those in the not ADNC group with respect to age, but there were more females than males in the high ADNC group and more males than females in the not ADNC group (Table 1).

CAA pathology is common in the occipital lobe [3] and historically is graded in this region in the UW NP Core. Specifically, using histochemical and immunohistochemical assessments, CAA is judged as absent with

no labeling, mild if the CAA is limited to leptomeningeal vessels, moderate if a minority of penetrating cortical arterioles are positive, and severe if a majority of penetrating arterioles are involved. Accordingly, for the CAA-focused portion of the study we chose to examine occipital cortex as neuropathologic assessments for CAA were performed in these tissue samples, and this is a region well-suited to capturing the neuropathologic changes of CAA [9]. Cases were selected based on the level of CAA in subjects with no Lewy body disease and no more than 1 microinfarct. Since CAA neuropathology is usually accompanied by ADNC, levels of CAA and ADNC in the CAA samples were classified (as follows): “no CAA/not ADNC” ($n=14$ FFPE/14 frozen); “moderate-severe CAA/intermediate-high ADNC” ($n=26$ FFPE/26 frozen) using an adaptation of, and in alignment with, NIA-AA guidelines [32]. Female/male representation was 50% in the CAA groups with an age range of 64–101 years (no CAA group) and 59–98 (moderate-severe CAA group). Patients in the moderate-severe CAA group did not differ significantly from those in the no CAA group with respect to sex or age (Table 1).

Immunohistochemistry (IHC)

The FFPE brain tissue samples described above were sectioned at 5 μ m, mounted on slides, deparaffinized, the antigens unmasked by heating to 100 $^{\circ}$ C in pH 6.0 citrate buffer (Item 3300, Vector Laboratories, Burlingame, CA), and endogenous peroxidases inactivated with 3% (v/v) H $_2$ O $_2$ in Tris-buffered saline. The sections were then blocked in 2% (v/v) normal goat serum. Subsequently, the sections were exposed to 1–5 μ g/mL of primary rabbit polyclonal antibodies (pAbs—all from Abcam, Cambridge, UK) that recognized human alpha-smooth muscle

actin (Item ab5694), PECAM/CD31 (Item ab28364), or von Willebrand factor (vWF) (Item ab6994). The latter two are specific markers for endothelial cells [33, 34]. Bound anti-alpha-smooth muscle actin pAb was visualized by immunofluorescence (IF), using Alexa-Fluor 594-goat anti-rabbit IgG (Item A11012, Thermo Fisher Scientific, Waltham, MA) in conjunction with 4',6-diamidino-2-phenylindole (DAPI) nuclear stain. Bound pAbs to vWF and PECAM were visualized chromogenically using biotinylated secondary antibodies in conjunction with Vectastain[®] Avidin–Biotin Complex (ABC) (Item PK-6105, Vector) and 3,3'-diaminobenzidine (DAB) (Item SK-4105, Vector). Cell nuclei were counterstained with hematoxylin. Labeled sections of the gray matter of the cortex were randomly selected, with no overlap, and imaged by a blinded observer with a Leica DMR epifluorescence microscope (Leica Microsystems, Wetzlar, Germany) equipped with a SPOT[™] 1.4 megapixel CCD camera (Diagnostic Instruments, Sterling Heights, MI) (for IF) and a Leica DM2500 microscope equipped with a SPOT Insight 4 megapixel color CCD camera (for brightfield).

Quantification of labeled brain sections

Paraffin sections representing each of the groups described in “Brain tissue samples” above were stained at the same time and under the same conditions using identical exposure parameters. MV density from digital photomicrographs (4 images per section) was quantified using ImageJ (National Institutes of Health image analysis freeware, <https://imagej.nih.gov/ij/>). Quantification was expressed as an “area fraction”; i.e., the area in μm^2 stained with MV markers (alpha-smooth muscle actin, PECAM, or vWF) divided by the area of the “standard” photomicrographic field ($4\text{ mm}^2 \times 100\%$) [35]. Measurement of MV luminal diameter (in μm) was performed by collecting digital images at $10\times$ magnification and measuring 4 vessels within each image (3 images per section).

Isolation of brain MV

Frozen samples of parietal cortex or occipital cortex (without meninges) were thawed and the grey matter dissected away from white matter. For each sample, the isolated grey matter was triturated in serum-free Dulbecco's Modified Eagle Medium (DMEM) with 4–5 strokes of a Dounce-type tissue grinder with a Teflon plunger. The triturated samples were centrifuged ($2000\times g$) at room temperature for 15 s, the supernatants discarded, and the vascular pellet was resuspended in DMEM. When necessary to remove large fragments and single cells, the suspension was filtered through $300\ \mu\text{m}$ and $30\ \mu\text{m}$ meshes, respectively. To eliminate debris: Dextran gradient isolation was done using 40% (w/v) dextran in isolation buffer

(DMEM low glucose with 1% Dextran) followed by centrifugation at $3000\times g$ for 15 min at $4\ ^\circ\text{C}$. Retentates were evaluated by phase contrast microscopy to confirm the presence of MV. The samples were then washed 3 times by centrifugation through cold PBS and either imaged by IF or lysed for polyacrylamide gel electrophoresis (PAGE)/western blot analysis (described below).

MV imaging by IF

A subset of isolated MV was fixed in neutral-buffered formalin, blocked in 2% goat serum, and exposed to rabbit pAbs recognizing human PECAM (Item ab28364, Abcam), vWF (Item ab6994, Abcam), PDGFRbeta (Item 3169S, Cell Signaling Technology), GFAP (Item ab7260, ABCAM), laminin (Item L9393, Millipore-Sigma, Burlington, MA), or col IV (Item ab6586, Abcam). Bound pAbs were visualized using Alexa-Fluor 594-goat anti-rabbit IgG. Cell nuclei were counterstained with DAPI. Labeled sections were imaged with the Leica DMR microscope/SPOT camera system described previously.

PAGE/western blot immunoassays

Isolated MV were lysed in M-PER[™] Mammalian Protein Extraction Reagent (Item78505, ThermoFisher) with protease inhibitors (Item78439, ThermoFisher). Total protein content of the lysates was measured by bicinchoninic acid assay. A portion ($20\ \mu\text{g}$ total protein) of each sample was reduced using NuPAGE[™] Sample Reducing Agent (ThermoFisher), resolved by PAGE, transferred to nitrocellulose, and probed with 2–5 $\mu\text{g}/\text{mL}$ of primary antibody as previously described [36]. Antibodies used were rabbit pAbs recognizing laminin (Item L9393, Millipore-Sigma), col IV (Item ab6586, Abcam), fibronectin (Item AB2033, Millipore-Sigma), or TSG-6 (RAH-1; [37]). A rat monoclonal antibody recognizing human HSPG2 (perlecan) (Item ab2501, Abcam) was also used. Primary antibodies bound to the blots were visualized with the appropriate horseradish peroxidase-conjugated secondary antibodies (Jackson Immuno Research, West Grove, PA) ($1\ \mu\text{g}/\text{mL}$), visualized by enhanced chemiluminescence (GE Healthcare Life Sciences, Pittsburgh, PA), scanned, and quantified using ImageJ as previously described [36].

HA ELISA

MV isolates were washed once with PBS and homogenized in PBS with a tissue homogenizer. An equal volume of Cell Lysis Buffer 2 (Item 895347, R&D Systems/Bio-Techne) was added and tissues were lysed. Debris was then removed by centrifugation. An aliquot of the lysate was removed and assayed to determine HA levels using a quantitative sandwich enzyme immunoassay technique with a Hyaluronan Quantikine ELISA kit (R&D Systems) per the manufacturer's instructions. HA content in the

samples was normalized to the total protein content of each sample.

Statistical analysis

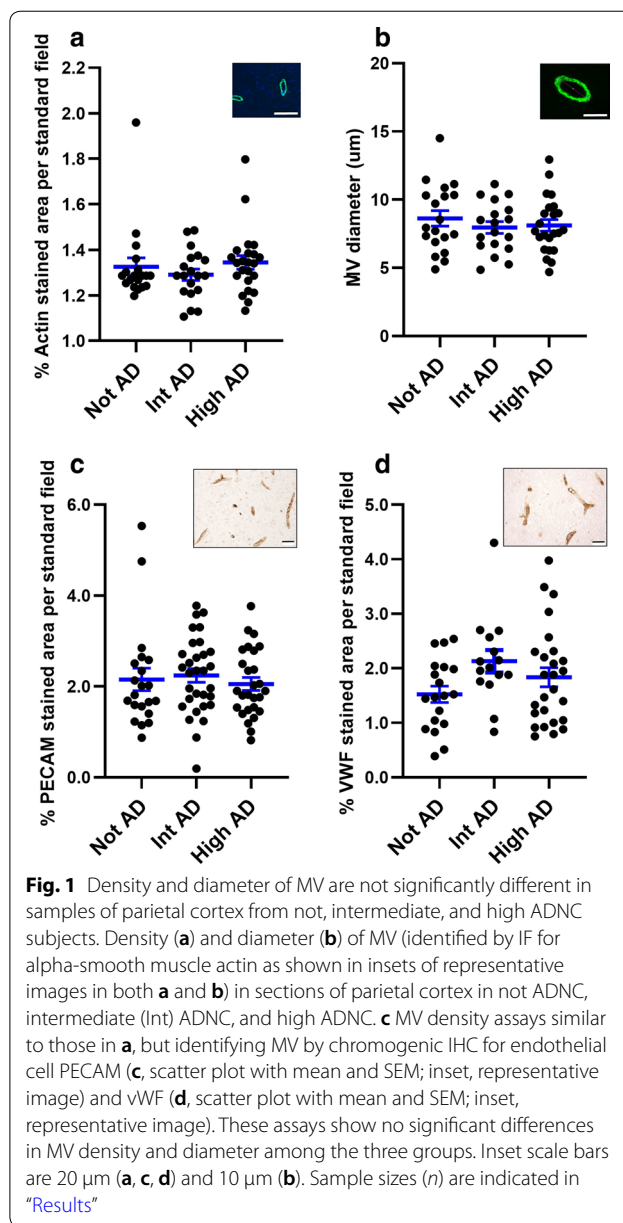
Initial comparisons for significant differences among not, intermediate and high ADNC for MV density were made by ANOVA. Significant differences between not versus high ADNC and no CAA versus moderate-severe CAA for MV density, basement membrane components, TSG-6, and HA content were then determined using a paired Student’s t-test with unequal variance. Statistical significance was defined as $p < 0.05$.

Results

The focus of this study was to characterize changes in MV density, MV diameter, and levels of key ECM components in brain samples exhibiting differing levels of ADNC or CAA neuropathology. Samples from the parietal lobe were selected to assess ADNC, as described in “Methods”. Samples from the occipital lobe were selected to assess CAA, as described in “Methods”. Grading was confirmed by a board-certified neuropathologist at the original autopsy, using appropriate criteria.

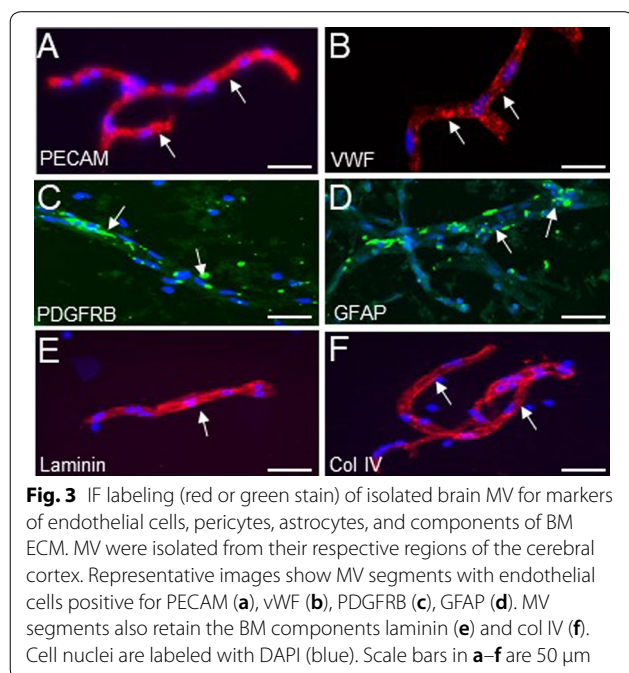
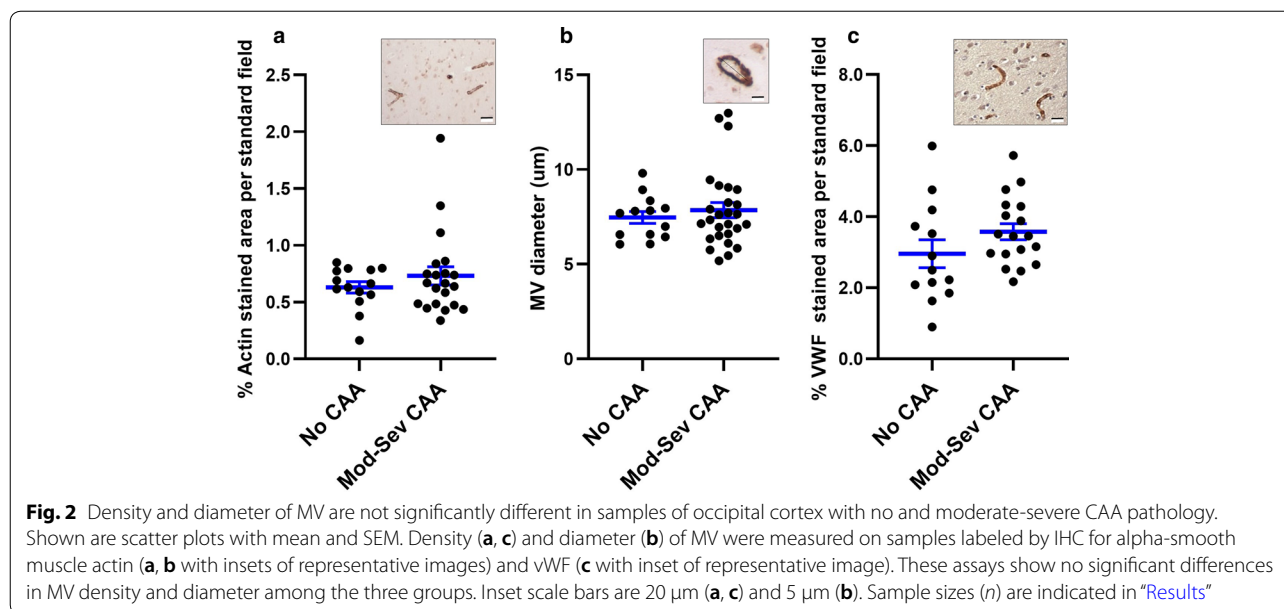
The cortical thickness of the specimens was measured to confirm that there were no significant differences in cortical atrophy among the samples obtained from each of the groups (data not shown). Initial experiments examined the organization of MV in sections from the AD brain samples (not ADNC, intermediate ADNC, or high ADNC groups). Analysis of MV by IHC was limited to areas at least 100 μm from an amyloid plaque. Alpha-smooth muscle actin staining of microvasculature showed that there were no significant differences in MV density (Fig. 1a) or diameter (Fig. 1b) among the three groups ($n=19$ not ADNC, $n=15$ intermediate ADNC, and $n=23$ high ADNC). IHC for endothelial cell PECAM (Fig. 1c) and vWF (Fig. 1d) to mark MV also revealed no differences in MV density among the groups (for PECAM staining: $n=19$ not ADNC, $n=15$ intermediate ADNC, $n=39$ high ADNC; for vWF staining: $n=10$ not ADNC, $n=9$ intermediate ADNC, $n=17$ high ADNC). In parallel experiments, we found no significant differences in MV density in frontal lobe cortex samples from not-, intermediate-, and high ADNC groups, as assayed by IHC for alpha-smooth muscle actin ($n=5$ for each group) and PECAM ($n=10$ for each group) (data not shown).

Similar assays were performed on sections from the no CAA and moderate-severe CAA groups. Alpha-smooth muscle actin staining showed that there were no significant differences in MV density (Fig. 2a) or diameter (Fig. 2b) between the groups ($n=13$ no CAA, $n=22$ moderate-severe CAA). IHC for VWF (Fig. 2c) to mark



MV also revealed no differences in MV density among the groups ($n=13$ no CAA and $n=22$ moderate-severe CAA).

In subsequent experiments, we assessed the relative expression of major BM components of MV isolated from frozen AD or CAA samples (each frozen sample had a corresponding FFPE sample that had been assessed by IHC). The isolated MV were confirmed to be vasculature by morphology and by IF assay for expression of PECAM (Fig. 3a) and VWF (Fig. 3b). The MV contained components of pericytes (Fig. 3c) and astrocytes (Fig. 3d)



as well as the BM, as shown by IF for laminin (Fig. 3e) and col IV (Fig. 3f).

The isolated MV from the AD and CAA brain samples were then subjected to PAGE/western blot immunoassay and HA ELISA to assess the levels of key ECM components. With respect to the AD samples (obtained from the parietal lobe), the ECM proteins laminin (Fig. 4a) and col IV (Fig. 4b) were significantly lower in MV from high ADNC brains relative to not ADNC brains ($n=12$

per group, laminin $p=0.02$ and col IV $p=0.03$). In contrast, the expression of fibronectin and perlecan were not significantly different between the high ADNC and not ADNC groups (data not shown). We have previously shown that high ADNC samples have significantly higher TSG-6 and HA content relative to not ADNC samples [31].

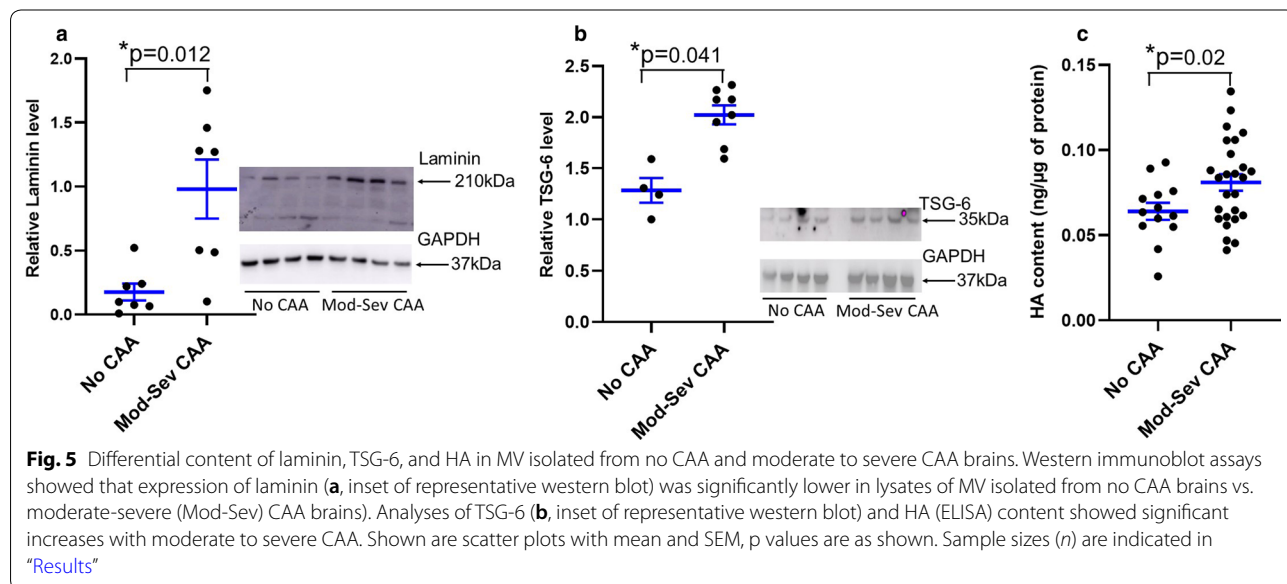
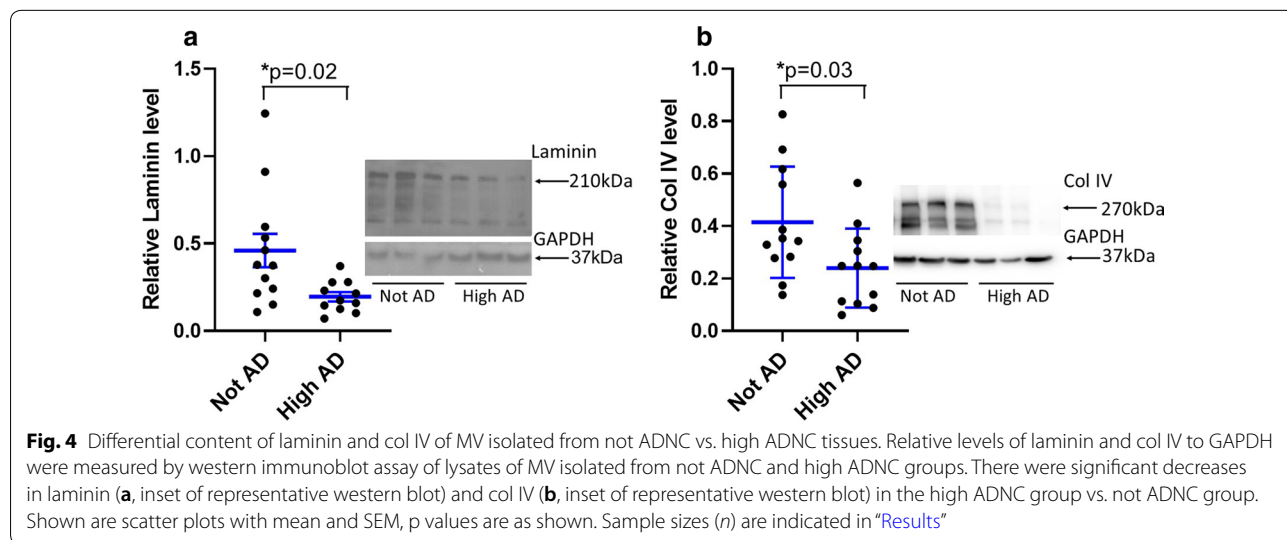
In studies of the CAA samples (no CAA, $n=7$; moderate-severe CAA, $n=7$), expression of laminin (Fig. 5a) was significantly higher in MV from moderate-severe CAA brains vs. the no CAA brains ($p=0.012$)—a trend that was opposite to that seen in the ADNC samples, where laminin expression decreased coincidentally with ADNC (Fig. 4a). The decrease in expression of laminin was supported by studies with a specific antibody against alpha 5 laminin (Invitrogen MA5-24649, data not shown). With the number of samples available, we were not able to detect differences in col IV, fibronectin, or perlecan (data not shown). However, TSG-6 (Fig. 5b) and HA (Fig. 5c) levels were both significantly higher in moderate-severe CAA brains ($n=8$ for western blot and $n=26$ for HA ELISA) vs no CAA brains ($n=4$ for western blot and $n=14$ for HA ELISA), which was similar to what we have previously found in high ADNC vs not ADNC [31].

Discussion

The microvasculature of the brain is a dynamic network that regulates blood flow to meet the high metabolic needs of neurons. Prior studies measuring AD-associated changes in MV density or morphology reported increased MV density in AD brains relative to age-matched control brains [11, 38, 39], but other studies

have reported a lower MV density in AD brains compared to control brains [40]. Studies of changes in MV in CAA brains are not as plentiful as corresponding studies of AD, and the CAA studies also report conflicting data [3, 16]. Analysis of the status of MV in CAA is further complicated by the fact that CAA pathology varies by brain region in a manner that does not always correlate with the pathologic changes of AD. In contrast to previous studies, our data indicate that in the absence of chronic vascular brain injury and Lewy body pathology, there are no significant differences in MV density or diameter in parietal or frontal cortex tissues with high ADNC relative to intermediate AD and not ADNC brain

samples. Similarly, MV density and diameter do not differ in occipital cortex of brains with moderate-severe CAA vs. no CAA. Our results reflect analyses of three different markers of MV. The conflicting data reported by prior studies could reflect, in part, the impact of cortical atrophy, which can be seen in association with a variety of pathologies including AD and vascular brain injury. Loss of brain volume due to atrophy, which is difficult to measure in isolated portions of brain samples, could mask a decrease in MV density. Additional variability in measures of MV density could arise in areas of inflammation, such as near amyloid plaques. Both of these variables were accounted for in our analyses.



The BM of the MV contributes to the integrity of the blood–brain barrier (BBB) [13]. The BBB (comprised of brain endothelial cells tightly associated with pericytes, astrocyte end feet, the glycocalyx, and the BM) restricts the passage of intravascular contents into the brain parenchyma [14, 41–43]. The BM is sometimes described as having endothelial and parenchymal layers, which are constituted from sequential deposition of structural and regulatory ECM [13, 44]. The ECM responds to forces from both the luminal and abluminal (parenchymal) side via integrins and other ECM-binding cell surface receptors. As a consequence, it is generally accepted that BM thickening, largely due to changes in laminin and col IV, occurs in the microvasculature throughout the body in response to chronic stresses, such as shear forces, high pressures, and aging [7, 16, 45, 46]. Accordingly, it is reasonable to predict that the thickness and ECM composition of the BM would change in brain MV in the presence of high ADNC or severe CAA neuropathology.

In the present study, we found that laminin was significantly lower in lysates of MV isolated from high ADNC vs. not ADNC brains. Our data are based on what is generally considered a pan laminin antibody [47, 48], but few prior studies have specifically examined laminin in the BBB with neurodegeneration. Early work reported an increase in punctate deposits of $\alpha 1$ and $\gamma 1$ laminin chains in plaques of A β and in astrocytes of human brain parenchyma [49]. In IHC studies of Braak stage III–VI AD patients relative to age-matched controls, laminin exhibited patterns indicating BM fragmentation in AD and co-localized with A β in senile plaques, which could reflect a net decrease in intact laminin with AD [50]. We also found that col IV was lower in MV lysates from high ADNC vs. not ADNC tissues. Other studies of changes in col IV with AD have shown variable results. Early studies reported a 55% increase in col IV content in the cerebral MV of AD patients compared to controls [51]. Additional investigations of the brains of AD patients have reported a thickening of the BM together with an increase in collagen content [52–55]. Moreover, a recent study reported that MV of frontal and temporal cortex of subclinical AD and AD groups had significantly higher levels of col IV staining than a control group [18]. In contrast (and similar to our findings), Christov et al. reported that col I and III increased, but col IV decreased, in MV from AD subjects relative to MV from healthy controls [15]. Fibronectin is a large glycoprotein that exists in a soluble form in the plasma, and is a ubiquitous insoluble dimer in most tissues [56]. Recent IHC studies demonstrate that cellular fibronectin staining is highly variable, with an increase noted in frontal cortex, but not temporal cortex, in AD brains relative to age-matched controls [18]. These data are consistent with our observation, in

western immunoblots, of no detectable differences in fibronectin content in MV isolated from high AD vs. not AD parietal cortex. We also did not find AD-related changes in the HSPG perlecan, which is present in low levels in MV [17]. Correspondingly, earlier investigations found no significant difference in perlecan mRNA levels in tissue of the hippocampus of AD patients when compared to age-matched controls [57]. Recent IHC studies suggest perlecan and other HSPGs are increased in AD, which correlates with increased staining for A β [18, 58].

In contrast to the cases studied for ADNC, we found that laminin content was significantly higher in lysates of MV isolated from moderate-severe CAA vs. no CAA brains. We could not detect differences in col IV, perlecan, or fibronectin, which could reflect the limited number of CAA samples that were available. Of note, the higher level of MV-associated laminin in the presence of vascular A β deposition due to CAA is consistent with other processes that induce tension and BM thickening in vasculature [44, 59]. The presence of CAA may promote the deposition of ECM as a generalized response to stress on the BM. Conversely, we find microvasculature in the presence of high ADNC has a decrease in BM ECM content that could reflect a response to neuronal loss, pericyte drop-out and increased matrix metalloprotease activity [60, 61]. Conflicting results obtained in efforts to quantify changes in ECM associated with development of brain pathology likely reflect: (1) differences in ECM composition between the different brain regions that were sampled, (2) variations in the local microenvironment of plaques and tangles within a specific brain region, and (3) differences in the methods or techniques utilized to measure specific ECM components. We note our sample numbers were constrained by the requirement to have minimal other vascular or neurodegenerative processes, and our results are limited to analyses of portions of brain cortex that are representative of ADNC or CAA, respectively. Nonetheless, these results indicate that measures of BM content in MV will reflect the dominant pathology in any given section of brain tissue, and underscore the fact that brain MV will have unique ECM compositions that are determined by their microenvironment.

Unlike BM ECM components, both TSG-6 and HA content are greater in moderate-severe CAA relative to no CAA, similar to the higher levels we previously found in high ADNC relative to no ADNC. These results are not surprising—HA is a prevalent non-sulfated GAG that increases in content during CNS aging and injury, including neurodegenerative processes [13, 35]. Structural and functional effects of HA are largely mediated by the hyaladherins to which it is bound [21, 62]. In the brain, HA is most highly associated with

chondroitin sulfate proteoglycans (CSPGs), but the inflammation-associated hyaladherin TSG-6 is also constitutively present, where it has been implicated in the organization of the HA matrix [27]. Complexes of HA and TSG-6 have enhanced binding to the HA receptor CD44 [29, 63]. This may explain how TSG-6 mediates some of its anti-inflammatory effects in a CD44 dependent manner [28, 64, 65]. Further studies are needed to determine whether the increase in HA and TSG-6 is a modulator in the microvascular response to AD and CAA, or represents a generalized response to injury.

Conclusion

In conclusion, we find that in the absence of significant vascular disease, the brains of subjects with ADNC vs. not ADNC and CAA vs. no CAA did not differ with respect to the density and diameter of MV. However, MV-associated BM was altered with lower levels of both laminin and col IV in the BM of MV isolated from high ADNC vs. not ADNC tissues, but higher levels of laminin in the BM of MV isolated from moderate-severe CAA vs. no CAA brains. Similar to ADNC, CAA MV have a higher amount of TSG-6 and HA. These data demonstrate that the general morphology of brain MV is not appreciably altered following development of ADNC or CAA, but there are notable changes in BM ECM content and increases in prevalent ECM components like HA, which could have disease and regional specific effects on microvascular function.

Acknowledgements

The authors thank Dr. Virginia M. Green for assistance with the manuscript, Drs. Thomas Wight, Ingrid Harten, Michelle Erickson, Aric Logsdon, and Kimberly Alonge for many helpful discussions, and Kim Hansen, Kim Howard and Allison Beller for technical and administrative support, respectively.

Authors' contributions

MD performed the microvessel isolations, the biochemistry experiments, analyzed the data, and developed all of the graphic data. RBV imaged, analyzed and interpreted the histologic data and assisted with writing the manuscript. JP performed and imaged the histologic experiments and analyzed the histologic data. CDK interpreted all the pathologic classifications and histologic data. AJD analyzed and interpreted the microvessel biochemistry data and was a major contributor with writing the manuscript. WAB interpreted the histologic and biochemical data and assisted with writing the manuscript. MJR analyzed and interpreted all the experimental data and was the primary writer of the manuscript. All authors read and approved the final manuscript.

Funding

This work was supported by the National Center for Advancing Translational Sciences of the National Institutes of Health under Award Number UL1 TR002319; NIH grants R03AG051071 and R21AG056883 (to M.J.R.), R01AG046619 (to W.A.B.); a major award from the Klorfine Foundation (R.B.V.); the VA (W.A.B.); and the Nancy and Buster Alvord Endowment (C.D.K.). The authors also thank the University of Washington Alzheimer's Disease Research Center (NIH P50 AG005136) and the Adult Changes in Thought Study (NIH U01 AG006781). The funding sources had no involvement in study design; in the collection, analysis and interpretation of data; in the writing of this article; or in the decision to submit this article for publication.

Availability of data and materials

The datasets during and/or analysed during the current study available from the corresponding author on reasonable request.

Ethics approval and consent to participate

De-identified human brain issues are provided by the University of Washington Alzheimer's Disease Research Center and the Adult Changes in Thought Study.

Consent for publication

Not applicable.

Competing interests

Anthony J. Day is a Director of Link Biologics, which is focused on the use of a TSG-6-based biological drug for inflammatory conditions. The other authors have no conflict of interest to report.

Author details

¹ Division of Gerontology and Geriatric Medicine, Department of Medicine, University of Washington, Seattle, WA, USA. ² Geriatric Research Education and Clinical Center, VA Puget Sound Health Care System, Seattle, WA, USA. ³ Matrix Biology Program, Benaroya Research Institute at Virginia Mason, Seattle, WA, USA. ⁴ Division of Neuropathology, Department of Pathology, University of Washington, Seattle, WA, USA. ⁵ Wellcome Trust Centre for Cell-Matrix Research and Lydia Becker Institute of Immunology and Inflammation, Division of Cell-Matrix Biology & Regenerative Medicine, School of Biological Sciences, Faculty of Biology, Medicine and Health, University of Manchester, Manchester Academic Health Sciences Centre, Manchester, UK. ⁶ Division of Gerontology and Geriatric Medicine, Department of Medicine, University of Washington Harborview Medical Center, Seattle, WA 98104, USA.

Received: 18 May 2020 Accepted: 9 September 2020

Published online: 29 September 2020

References

- Jack CR Jr, Bennett DA, Blennow K, Carrillo MC, Dunn B, Haeberlein SB, et al. NIA-AA research framework: toward a biological definition of Alzheimer's disease. *Alzheimers Dement*. 2018;14(4):535–62. <https://doi.org/10.1016/j.jalz.2018.02.018>.
- Montine TJ, Phelps CH, Beach TG, Bigio EH, Cairns NJ, Dickson DW, et al. National Institute on Aging-Alzheimer's Association guidelines for the neuropathologic assessment of Alzheimer's disease: a practical approach. *Acta Neuropathol*. 2012;123(1):1–11. <https://doi.org/10.1007/s00401-011-0910-3>.
- Biffi A, Greenberg SM. Cerebral amyloid angiopathy: a systematic review. *J Clin Neurol*. 2011;7(1):1–9. <https://doi.org/10.3988/jcn.2011.7.1.1>.
- Yamada M. Cerebral amyloid angiopathy: emerging concepts. *J Stroke*. 2015;17(1):17–30. <https://doi.org/10.5853/jos.2015.17.1.17>.
- Cargill R, Kohama SG, Struve J, Su W, Banine F, Witkowski E, et al. Astrocytes in aged nonhuman primate brain gray matter synthesize excess hyaluronan. *Neurobiol Aging*. 2012;33(4):830.e13–24. <https://doi.org/10.1016/j.neurobiolaging.2011.07.006>.
- Machin DR, Bloom SI, Campbell RA, Phuong TTT, Gates PE, Lesniewski LA, et al. Advanced age results in a diminished endothelial glycocalyx. *Am J Physiol Heart Circ Physiol*. 2018;315(3):H531–H539. <https://doi.org/10.1152/ajpheart.00104.2018>.
- Scioli MG, Bielli A, Arcuri G, Ferlosio A, Orlandi A. Ageing and microvasculature. *Vasc Cell*. 2014;6:19. <https://doi.org/10.1186/2045-824X-6-19>.
- Tucsek Z, Toth P, Tarantini S, Sosnowska D, Gautam T, Warrington JP, et al. Aging exacerbates obesity-induced cerebrovascular rarefaction, neurovascular uncoupling, and cognitive decline in mice. *J Gerontol A Biol Sci Med Sci*. 2014;69(11):1339–522. <https://doi.org/10.1093/gerona/glu080>.
- Kovari E, Herrmann FR, Hof PR, Bouras C. The relationship between cerebral amyloid angiopathy and cortical microinfarcts in brain ageing and Alzheimer's disease. *Neuropathol Appl Neurobiol*. 2013;39(5):498–509. <https://doi.org/10.1111/nan.12003>.
- Vasilevko V, Passos GF, Quiring D, Head E, Kim RC, Fisher M, et al. Aging and cerebrovascular dysfunction: contribution of hypertension,

- cerebral amyloid angiopathy, and immunotherapy. *Ann N Y Acad Sci.* 2010;1207:58–70. <https://doi.org/10.1111/j.1749-6632.2010.05786.x>.
11. Biron KE, Dickstein DL, Gopaul R, Jefferies WA. Amyloid triggers extensive cerebral angiogenesis causing blood brain barrier permeability and hypervascularity in Alzheimer's disease. *PLoS ONE.* 2011;6(8):e23789. <https://doi.org/10.1371/journal.pone.0023789>.
 12. Burke MJ, Nelson L, Slade JY, Oakley AE, Khundakar AA, Kalaria RN. Morphometry of the hippocampal microvasculature in post-stroke and age-related dementias. *Neuropathol Appl Neurobiol.* 2014;40(3):284–95. <https://doi.org/10.1111/nan.12085>.
 13. Reed MJ, Damodarasamy M, Banks WA. The extracellular matrix of the blood-brain barrier: structural and functional roles in health, aging, and Alzheimer's disease. *Tissue Barriers.* 2019;7(4):1651157. <https://doi.org/10.1080/21688370.2019.1651157>.
 14. Xu L, Nirwane A, Yao Y. Basement membrane and blood-brain barrier. *Stroke Vasc Neurol.* 2018;4(2):78–82.
 15. Christov A, Ottman J, Hamdheydari L, Grammas P. Structural changes in Alzheimer's disease brain microvessels. *Curr Alzheimer Res.* 2008;5(4):392–5.
 16. Hawkes CA, Gatherer M, Sharp MM, Dorr A, Yuen HM, Kalaria R, et al. Regional differences in the morphological and functional effects of aging on cerebral basement membranes and perivascular drainage of amyloid-beta from the mouse brain. *Aging Cell.* 2013;12(2):224–36. <https://doi.org/10.1111/acer.12045>.
 17. Hawkes CA, Hartig W, Kacza J, Schliebs R, Weller RO, Nicoll JA, et al. Perivascular drainage of solutes is impaired in the ageing mouse brain and in the presence of cerebral amyloid angiopathy. *Acta Neurobiol.* 2011;121(4):431–43. <https://doi.org/10.1007/s00401-011-0801-7>.
 18. Lepelletier FX, Mann DM, Robinson AC, Pinteaux E, Boutin H. Early changes in extracellular matrix in Alzheimer's disease. *Neuropathol Appl Neurobiol.* 2017;43(2):167–82. <https://doi.org/10.1111/nan.12295>.
 19. Simpson MA, de la Motte C, Sherman LS, Weigel PH. Advances in hyaluronan biology: signaling, regulation, and disease mechanisms. *Int J Cell Biol.* 2015;2015:690572. <https://doi.org/10.1155/2015/690572>.
 20. Dubacheva GV, Curk T, Auzely-Velty R, Frenkel D, Richter RP. Designing multivalent probes for tunable superselective targeting. *Proc Natl Acad Sci USA.* 2015;112(18):5579–84. <https://doi.org/10.1073/pnas.1500622112>.
 21. Richter RP, Baranova NS, Day AJ, Kwok JC. Glycosaminoglycans in extracellular matrix organisation: are concepts from soft matter physics key to understanding the formation of perineuronal nets? *Curr Opin Struct Biol.* 2018;50:65–74. <https://doi.org/10.1016/j.sbi.2017.12.002>.
 22. Al-Ahmad AJ, Patel R, Palecek SP, Shusta EV. Hyaluronan impairs the barrier integrity of brain microvascular endothelial cells through a CD44-dependent pathway. *J Cereb Blood Flow Metab.* 2018. <https://doi.org/10.1177/0271678X18767748>.
 23. Back SA, Tuohy TM, Chen H, Wallingford N, Craig A, Struve J, et al. Hyaluronan accumulates in demyelinated lesions and inhibits oligodendrocyte progenitor maturation. *Nat Med.* 2005;11(9):966–72. <https://doi.org/10.1038/nm1279>.
 24. Jiang D, Liang J, Noble PW. Hyaluronan as an immune regulator in human diseases. *Physiol Rev.* 2011;91(1):221–64. <https://doi.org/10.1152/physrev.00052.2009>.
 25. Misra S, Hascall VC, Markwald RR, Ghatak S. Interactions between hyaluronan and its receptors (CD44, RHAMM) regulate the activities of inflammation and cancer. *Front Immunol.* 2015;6:201. <https://doi.org/10.3389/fimmu.2015.00201>.
 26. Dong Y, Arif A, Olsson M, Cali V, Hardman B, Dosanjh M, et al. Endotoxin free hyaluronan and hyaluronan fragments do not stimulate TNF-alpha, interleukin-12 or upregulate co-stimulatory molecules in dendritic cells or macrophages. *Sci Rep.* 2016;6:36928. <https://doi.org/10.1038/srep36928>.
 27. Coulson-Thomas VJ, Lauer ME, Soleman S, Zhao C, Hascall VC, Day AJ, et al. Tumor necrosis factor-stimulated gene-6 (TSG-6) is constitutively expressed in adult central nervous system (CNS) and associated with astrocyte-mediated glial scar formation following spinal cord injury. *J Biol Chem.* 2016;291(38):19939–52. <https://doi.org/10.1074/jbc.M115.710673>.
 28. Day AJ, Milner CM. TSG-6: a multifunctional protein with anti-inflammatory and tissue-protective properties. *Matrix Biol.* 2019;78–79:60–83. <https://doi.org/10.1016/j.matbio.2018.01.011>.
 29. Baranova NS, Nileback E, Haller FM, Briggs DC, Svedhem S, Day AJ, et al. The inflammation-associated protein TSG-6 cross-links hyaluronan via hyaluronan-induced TSG-6 oligomers. *J Biol Chem.* 2011;286(29):25675–86. <https://doi.org/10.1074/jbc.M111.247395>.
 30. Watanabe J, Shetty AK, Hattiangady B, Kim DK, Foraker JE, Nishida H, et al. Administration of TSG-6 improves memory after traumatic brain injury in mice. *Neurobiol Dis.* 2013;59:86–99. <https://doi.org/10.1016/j.nbd.2013.06.017>.
 31. Reed MJ, Damodarasamy M, Pathan JL, Chan CK, Spiekerman C, Wight TN, et al. Increased Hyaluronan and TSG-6 in Association with Neuropathologic Changes of Alzheimer's Disease. *J Alzheimers Dis.* 2019;67(1):91–102. <https://doi.org/10.3233/JAD-180797>.
 32. Hyman BT, Phelps CH, Beach TG, Bigio EH, Cairns NJ, Carrillo MC, et al. National Institute on Aging-Alzheimer's Association guidelines for the neuropathologic assessment of Alzheimer's disease. *Alzheimers Dement.* 2012;8(1):1–13. <https://doi.org/10.1016/j.jalz.2011.10.007>.
 33. Iovino F, Molema G, Bijlsma JJ. Platelet endothelial cell adhesion molecule-1, a putative receptor for the adhesion of *Streptococcus pneumoniae* to the vascular endothelium of the blood-brain barrier. *Infect Immun.* 2014;82(9):3555–666. <https://doi.org/10.1128/IAI.00046-14>.
 34. Yamagata K, Matsumura K, Inoue W, Shiraki T, Suzuki K, Yasuda S, et al. Coexpression of microsomal-type prostaglandin E synthase with cyclooxygenase-2 in brain endothelial cells of rats during endotoxin-induced fever. *J Neurosci.* 2001;21(8):2669–777.
 35. Reed MJ, Damodarasamy M, Pathan JL, Erickson MA, Banks WA, Vernon RB. The effects of normal aging on regional accumulation of hyaluronan and chondroitin sulfate proteoglycans in the mouse brain. *J Histochem Cytochem.* 2018;66(10):697–707. <https://doi.org/10.1369/0022155418774779>.
 36. Reed MJ, Ferara NS, Vernon RB. Impaired migration, integrin function, and actin cytoskeletal organization in dermal fibroblasts from a subset of aged human donors. *Mech Ageing Dev.* 2001;122(11):1203–20.
 37. Fujimoto T, Savani RC, Watari M, Day AJ, Strauss JF 3rd. Induction of the hyaluronic acid-binding protein, tumor necrosis factor-stimulated gene-6, in cervical smooth muscle cells by tumor necrosis factor-alpha and prostaglandin E(2). *Am J Pathol.* 2002;160(4):1495–502. [https://doi.org/10.1016/s0002-9440\(10\)62575-8](https://doi.org/10.1016/s0002-9440(10)62575-8).
 38. Bennett RE, Robbins AB, Hu M, Cao X, Betensky RA, Clark T, et al. Tau induces blood vessel abnormalities and angiogenesis-related gene expression in P301L transgenic mice and human Alzheimer's disease. *Proc Natl Acad Sci USA.* 2018;115(6):E1289–E12981298. <https://doi.org/10.1073/pnas.1710329115>.
 39. Bouras C, Kovari E, Herrmann FR, Rivara CB, Bailey TL, von Gunten A, et al. Stereologic analysis of microvascular morphology in the elderly: Alzheimer disease pathology and cognitive status. *J Neuropathol Exp Neurol.* 2006;65(3):235–44. <https://doi.org/10.1097/01.jnen.0000203077.53080.2c>.
 40. Brown WR, Thore CR. Review: cerebral microvascular pathology in ageing and neurodegeneration. *Neuropathol Appl Neurobiol.* 2011;37(1):56–74. <https://doi.org/10.1111/j.1365-2990.2010.01139.x>.
 41. Erickson MA, Banks WA. Neuroimmune axes of the blood-brain barriers and blood-brain interfaces: bases for physiological regulation, disease states, and pharmacological interventions. *Pharmacol Rev.* 2018;70(2):278–314. <https://doi.org/10.1124/pr.117.014647>.
 42. Gastfriend BD, Palecek SP, Shusta EV. Modeling the blood-brain barrier: beyond the endothelial cells. *Curr Opin Biomed Eng.* 2018;5:6–12. <https://doi.org/10.1016/j.cobme.2017.11.002>.
 43. Sweeney MD, Kisler K, Montagne A, Toga AW, Zlokovic BV. The role of brain vasculature in neurodegenerative disorders. *Nat Neurosci.* 2018;21(10):1318–31. <https://doi.org/10.1038/s41593-018-0234-x>.
 44. Thomsen MS, Routh LJ, Moos T. The vascular basement membrane in the healthy and pathological brain. *J Cereb Blood Flow Metab.* 2017;37(10):3300–17. <https://doi.org/10.1177/0271678X17722436>.
 45. Kurtz A, Oh SJ. Age related changes of the extracellular matrix and stem cell maintenance. *Prev Med.* 2012;54(Suppl):S50–S5656. <https://doi.org/10.1016/j.jpmed.2012.01.003>.
 46. Uspenskaia O, Liebetrau M, Herms J, Daneke A, Hamann GF. Aging is associated with increased collagen type IV accumulation in the basal lamina of human cerebral microvessels. *BMC Neurosci.* 2004;5:37. <https://doi.org/10.1186/1471-2202-5-37>.
 47. Freeman R, Stephanopoulos N, Alvarez Z, Lewis JA, Sur S, Serrano CM, et al. Instructing cells with programmable peptide DNA hybrids. *Nat Commun.* 2017;8:15982. <https://doi.org/10.1038/ncomms15982>.

48. Li S, Haigh K, Haigh JJ, Vasudevan A. Endothelial VEGF sculpts cortical cytoarchitecture. *J Neurosci*. 2013;33(37):14809–15. <https://doi.org/10.1523/JNEUROSCI.1368-13.2013>.
49. Palu E, Liesi P. Differential distribution of laminins in Alzheimer disease and normal human brain tissue. *J Neurosci Res*. 2002;69(2):243–56. <https://doi.org/10.1002/jnr.10292>.
50. Berzin TM, Zipser BD, Rafii MS, Kuo-Leblanc V, Yancopoulos GD, Glass DJ, et al. Agrin and microvascular damage in Alzheimer's disease. *Neurobiol Aging*. 2000;21(2):349–55.
51. Kalara RN, Pax AB. Increased collagen content of cerebral microvessels in Alzheimer's disease. *Brain Res*. 1995;705(1–2):349–52.
52. Challa VR, Thore CR, Moody DM, Anstrom JA, Brown WR. Increase of white matter string vessels in Alzheimer's disease. *J Alzheimers Dis*. 2004;6(4):379–83.
53. Farkas E, De Jong GI, de Vos RA, Jansen Steur EN, Luiten PG. Pathological features of cerebral cortical capillaries are doubled in Alzheimer's disease and Parkinson's disease. *Acta Neuropathol*. 2000;100(4):395–402.
54. Tong XK, Nicolakakis N, Kocharyan A, Hamel E. Vascular remodeling versus amyloid beta-induced oxidative stress in the cerebrovascular dysfunctions associated with Alzheimer's disease. *J Neurosci*. 2005;25(48):11165–74. <https://doi.org/10.1523/JNEUROSCI.4031-05.2005>.
55. Zarow C, Barron E, Chui HC, Perlmutter LS. Vascular basement membrane pathology and Alzheimer's disease. *Ann NY Acad Sci*. 1997;826:147–60.
56. Maurer LM, Ma W, Mosher DF. Dynamic structure of plasma fibronectin. *Crit Rev Biochem Mol Biol*. 2015;51(4):213–27. <https://doi.org/10.1080/10409238.2016.1184224>.
57. Maresh GA, Erezylmaz D, Murry CE, Noehlin D, Snow AD. Detection and quantitation of perlecan mRNA levels in Alzheimer's disease and normal aged hippocampus by competitive reverse transcription-polymerase chain reaction. *J Neurochem*. 1996;67(3):1132–44.
58. Zhang GL, Zhang X, Wang XM, Li JP. Towards understanding the roles of heparan sulfate proteoglycans in Alzheimer's disease. *Biomed Res Int*. 2014;2014:516028. <https://doi.org/10.1155/2014/516028>.
59. Keable A, Fenna K, Yuen HM, Johnston DA, Smyth NR, Smith C, et al. Deposition of amyloid beta in the walls of human leptomeningeal arteries in relation to perivascular drainage pathways in cerebral amyloid angiopathy. *Biochim Biophys Acta*. 2016;1862(5):1037–46. <https://doi.org/10.1016/j.bbadis.2015.08.024>.
60. Halliday MR, Rege SV, Ma Q, Zhao Z, Miller CA, Winkler EA, et al. Accelerated pericyte degeneration and blood-brain barrier breakdown in apolipoprotein E4 carriers with Alzheimer's disease. *J Cereb Blood Flow Metab*. 2016;36(1):216–27. <https://doi.org/10.1038/jcbfm.2015.44>.
61. Rivera S, Garcia-Gonzalez L, Khrestchatsky M, Baranger K. Metalloproteinases and their tissue inhibitors in Alzheimer's disease and other neurodegenerative disorders. *Cell Mol Life Sci*. 2019;76(16):3167–91. <https://doi.org/10.1007/s00018-019-03178-2>.
62. Day AJ, Prestwich GD. Hyaluronan-binding proteins: tying up the giant. *J Biol Chem*. 2002;277(7):4585–8. <https://doi.org/10.1074/jbc.R100036200>.
63. Lesley J, Gal I, Mahoney DJ, Cordell MR, Rugg MS, Hyman R, et al. TSG-6 modulates the interaction between hyaluronan and cell surface CD44. *J Biol Chem*. 2004;279(24):25745–54. <https://doi.org/10.1074/jbc.M313319200>.
64. Choi H, Lee RH, Bazhanov N, Oh JY, Prockop DJ. Anti-inflammatory protein TSG-6 secreted by activated MSCs attenuates zymosan-induced mouse peritonitis by decreasing TLR2/NF-kappaB signaling in resident macrophages. *Blood*. 2011;118(2):330–8. <https://doi.org/10.1182/blood-2010-12-327353>.
65. Liu Y, Zhang R, Yan K, Chen F, Huang W, Lv B, et al. Mesenchymal stem cells inhibit lipopolysaccharide-induced inflammatory responses of BV2 microglial cells through TSG-6. *J Neuroinflamm*. 2014;11:135. <https://doi.org/10.1186/1742-2094-11-135>.

Publisher's Note

Springer Nature remains neutral with regard to jurisdictional claims in published maps and institutional affiliations.

Ready to submit your research? Choose BMC and benefit from:

- fast, convenient online submission
- thorough peer review by experienced researchers in your field
- rapid publication on acceptance
- support for research data, including large and complex data types
- gold Open Access which fosters wider collaboration and increased citations
- maximum visibility for your research: over 100M website views per year

At BMC, research is always in progress.

Learn more biomedcentral.com/submissions

